International Journal of Applied Earth Observations and Geoinformation 102 (2021) 102433

Contents lists available at ScienceDirect

International Journal of Applied Earth Observations and Geoinformation

journal homepage: www.elsevier.com/locate/jag

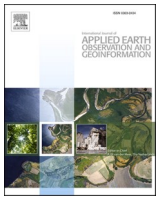

High-resolution sea level change around China seas revealed through multi-satellite altimeter data

Jiajia Yuan [a], Jinyun Guo [a,*], Chengcheng Zhu [a], Cheinway Hwang [b], Daocheng Yu [b], Mingzhi Sun [a], Dapeng Mu [c]

[a] College of Geodesy and Geomatics, Shandong University of Science and Technology, Qingdao 266590, China
[b] Department of Civil Engineering, National Chiao Tung University, Hsinchu, Taiwan
[c] Institute of Space Sciences, Shandong University, Weihai 264209, China

ARTICLE INFO

Keywords:
Sea level rise
Mean sea surface
Satellite altimeter
Sea surface height
Sentinel-3A
HY-2A

ABSTRACT

Sea level change is not uniform across the oceans and high-resolution sea level trend (SLT) models reveal that the rate of sea level change differs between different waters. In this study, we developed a new method for obtaining a high-resolution, 1′×1′-grid SLT model, using the time-varying mean sea surface (MSS) of several MSSs calculated from averaged multi-satellite-derived sea surface heights (TOPEX/Poseidon, Jason-1/2/3, ERS-1/2, Envisat, GFO, Cryosat-2, SARAL/AltiKa, Sentinel-3A, HY-2A) over different periods. We applied this model to estimate the mean sea level change in the China seas and their adjacent ocean (0°–41°N, 100°–140°E). This new model revealed the patterning of sea level change within the study region in detail, and detected a sea level change dipole south of Japan. A zonal SLT pattern was identified in three regions: the region of the North Pacific Subtropical Counter Current (an eastward current located in the band of 19.5°–22.5°N, populated with eddies), and the areas east of Taiwan and east of Luzon Island. Moreover, the rate of sea level rise in the offshore zone was found to be ~ 0.67 mm/yr (20%) higher than that in the open ocean. This finding has important implications for coastal protection.

1. Introduction

The global ocean, which accounts for 71% of the Earth's surface, plays a key role in the global climate change. Sea level changes are an important indicator of global climate change (Cazenave et al., 2014; Elipot 2020). The global mean sea level (GMSL) has been rising mainly due to global warming caused by the greenhouse effect (Church et al., 2001; Intergovernmental Panel on Climate Change (IPCC), 2014). Ongoing sea level rise (SLR) will cause considerable damage to the global economy and coastal cities, and directly threaten the development and even the survival of humankind (Nicholls and Cazenave, 2010; Nicholls et al., 2011; Niu et al., 2020).

Since the late 1960s, the GMSL has been rising continuously at an accelerating rise (Church and White, 2006; Watson et al., 2015; Watson, 2016; Mu and Yan, 2018; Voosen, 2020). Satellite altimeter data show that the rate of GMSL rise is approximately 3.3 mm/yr after correcting for interannual variability (Cazenave et al., 2014). Data from the last decade suggest that meltwater from the Greenland ice sheet has propelled the rate of SLR to 4.8 mm/yr with few signs of slowing down (Voosen, 2020). The rate of sea level change is not uniform across the global ocean, but differs between different waters (Nicholls and Cazenave, 2010; Guo et al., 2015; Mu and Yan, 2018; Voosen, 2020). For example, the average rate of SLR in the four China seas (South China, East China, Yellow, and Bohai Sea) between 1993 and 2012, estimated from the altimeter data of TOPEX/Poseidon (T/P), Jason-1 and Jason-2, was approximately 4.64 mm/yr—faster than the global mean rate (Guo et al., 2015). Moreover, this rate differed across the four China seas. In the tropical Pacific region along the U.S. west coast, however, sea level dropped at a rate of 3–5 mm/yr between 1993 and 2009 (Nicholls and Cazenave, 2010). There is, therefore, an urgent need for a high-resolution sea level trend (SLT) model that can resolve fine-scale sea level change in different seas. Such a model can provide important insights into the mechanisms of regional sea level change.

SLTs are usually obtained through least-square fitting to tide gauges or satellite altimetry observation time series (Mu and Yan, 2018), and represents the average sea level change trend in the study area during

* Corresponding author.
E-mail address: guojy@sdust.edu.cn (J. Guo).

https://doi.org/10.1016/j.jag.2021.102433
Received 3 March 2021; Received in revised form 28 June 2021; Accepted 2 July 2021
Available online 9 July 2021

the period of observation. SLT estimations are affected not only by the period of observation, but also by interannual changes in sea level mainly caused by El Niño–Southern Oscillation (Cazenave et al., 2014). For instances, the rate of GMSL rise dropped from 3.5 mm/yr in 2002 to approximately 2.5 mm/yr in 2008; after correcting for interannual variability; however, this slowdown in GMSL rise disappeared (Cazenave et al., 2014). This demonstrates that data post-processing, such as correcting for interannual sea level change, is essential for the accurate estimation of the rate of SLR.

With the development of satellite altimetry technology, satellite missions such as ERS-1/2, T/P, Jason-1/2/3, Geosat Follow On (GFO), Envisat, ICESat, Cryosat-2, SARAL/Altika (SRL), HY-2A, and Sentinel-3A, have collected abundant altimetric data, including exact repeat mission (ERM: e.g., T/P) and geodetic mission (GM: e.g., ERS-1/168) data. These datasets can be merged to derive a high-resolution (e.g., 1′×1′) mean sea surface (MSS) models (Jiang et al., 2002; Jin et al., 2011; Schaeffer et al., 2012; Jin et al., 2016; Pujol et al., 2018; Yuan et al., 2020a), such as the global MSS models CNES_CLS11 (Schaeffer et al., 2012), CNES_CLS15 (Pujol et al., 2018), DTU15 (Andersen et al., 2016), and DTU18 (Andersen et al., 2018). The MSS is the average sea surface height (SSH) derived from altimeter satellites over the observation period; therefore, it does not contain sea level change information (e.g., interannual variability). This information, nevertheless, can be obtained from MSS models by averaging the SSHs over different observation periods. For example, assuming that MSS models A, B, and C are the average SSHs for 1993–2012, 1994–2013, and 1995–2014, respectively, there is one year of sea level change information between models A and B, and B and C. Since the mean SSH of models A, B, and C changes over time, these models are referred to as time-varying MSSs.

Based on this background, here, we develop a new sea level modelling approach that uses time-varying MSSs, constructed from multi-satellite altimeter data, to derive an SLT model with an 1′×1′ grid, and apply this model to estimate the sea level change in the China seas and its adjacent ocean (CSO: 0°–41°N, 100°–140°E). We demonstrate that this model can accurately represent the spatial distribution characteristics of sea level change in the CSO. Besides the introduction, this paper is composed of the following three sections. Section 2 introduces data sources, and section3 introduces methodology. Section 4 presents the results and analysis, especially the SLT model on a 1′×1′ grid in the CSO. Section 5 presents the conclusions of this study.

2. Data sources

The satellite altimeter mission data used in this study were derived from the along-track Level-2+ (L2P) products released by Archiving Validation and Interpretation of Satellite Oceanographic Data (AVISO). These missions included ERS-1/2, T/P, Jason-1/2/3, Envisat, GFO, Cryosat-2, SRL, HY-2A, and Sentinel-3A. These missions data were 1-Hz along-track sea level data corrected for various errors (instrument errors, environmental perturbations, ocean sea state bias, atmospheric pressure, and the tide effect). These corrections are detailed in the along-track L2P product handbook (CNES, 2017).

Multi-satellite altimeter data from January 1993 to December 2019 in the CSO region were selected, as shown in Fig. 1. To reduce the contamination of the data by seasonal ocean changes and interannual signals, ERM data for the entire year were selected as much as possible (Schaeffer et al., 2012; Pujol et al., 2018; Yuan et al., 2020a). Moreover, to improve the spatial resolution of the MSS model, GM data, including ERS-1/GM, Jason-1/GM, HY-2A/GM, Cryosat-2, and SRL/drifting phase (DP), were also used.

Some other data products were also used for verification: these included the delayed-time gridded monthly mean of sea level anomalies, estimated from multi-satellite altimeter data from January 1993–September 2019 (AVISO); the SLT models with a 30′×30′ and 60′×60′ grid, by the National Oceanographic and Atmospheric Administration's (NOAA) Laboratory for Satellite Altimetry and the Commonwealth Scientific and Industrial Research Organization (CSIRO), and the altimeter data of T/P and Jason-1/2/3 over December 1992–September 2020 and January 1993–December 2019, respectively.

3. Methodology

We developed a new method for deriving sea level change, and for mapping the SLT in the CSO on a 1′×1′ grid. The multi-satellite altimeter

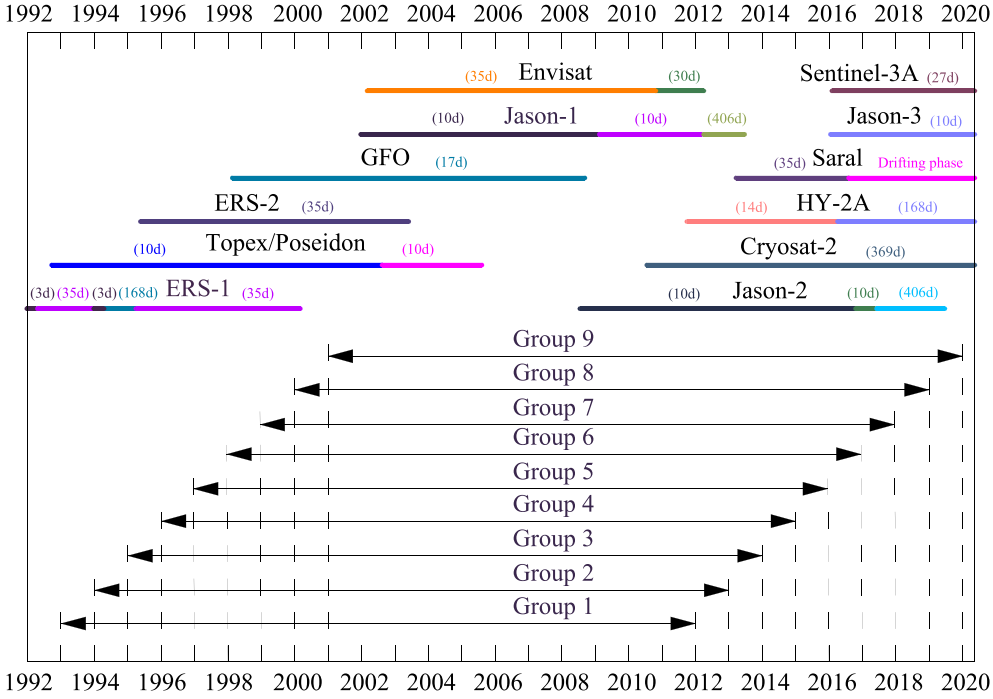

Fig. 1. Multi-satellite altimeter data from January 1993 to December 2019, grouped into 19-year-long moving windows shifted by one year (start date: January 1993). (Note: The contents in parentheses represent the repeated cycle of the altimeter mission).

data from January 1993 to December 2019 were divided into nine groups (Fig. 1). An MSS model with a 1′×1′ grid was then established separately for each group. Nine MSS models with the same grid size were thus obtained. These MSS models, corresponding to different periods of observation, form a time-varying MSS, which was used to derive a high-resolution SLT model. The data processing process included three main steps: 1) data grouping, 2) establishment of the MSS models, and, 3) construction of the grid model of the SLT.

3.1. Data grouping

Fig. 1 shows the nine multi-satellite altimeter datasets grouped into 19-year-long moving windows starting in January 1993 and shifting by one year. A one-year interval was present between adjacent datasets, as well as between the MSS models interpolated from these datasets.

As shown in Fig. 1, each group contained different satellite altimeter data; however, the altimeter data of the T/P series (T/P, Jason-1/2/3) were continuous within each group. The mean along-track SSHs of the uninterrupted joint T/P series were used as the fundament for establishing the MSS model in the next step of model development. These SSHs also served as a reference for calculating sea level anomalies, which were used for ocean variability correction. However, the period of the fundament different between the different groups: for instance, the period of Group1 was from January 1993 to December 2011, whereas that of Group 2 was from January 1994 to December 2012.

3.2. MSS model establishing

To obtain a high-resolution SLT model, a high-resolution MSS model must first be established. The MSS model obtained by interpolating the multi-satellite altimeter data was subjected to several procedures of data processing (Yuan et al., 2020a; 2020b), including the unification of reference ellipsoid, ocean variability correction, crossover adjustment, and gridding (Fig. 2).

The satellite-derived SSH is the distance between the sea surface and the surface of the reference ellipsoid. However, different altimeter satellites use different earth ellipsoid parameters; the SSHs derived from different satellite missions differed as a result. Before the multi-satellite altimeter data can be integrated to determine an MSS model, the satellite-derived SSHs must to be unified in relation to the same reference ellipsoid. Because the L2P satellite mission data were unified in relation to the same reference ellipsoid as that used in T/P (CNES, 2017), the establishing of an MSS model in this study consisted of three main data processing procedures: ocean variability correction, crossover adjustment, and gridding.

3.2.1. Ocean variability correction

The ocean variability correction refers to the correction of the ERM and GM data for temporal variation. Because the ground tracks of altimeter satellite with ERM are coinciding with each other, the correction of the ERM data for ocean variability can be done though collinear adjustment (Rapp et al., 1994; Jiang et al., 2002; Jin et al., 2011). Collinear adjustment was used to reduce the anomalous temporal variation in SSH caused by large-scale ocean anomalies (such as El Niño/La Niña) in a specific period and to obtain the mean along-track SSH (Jiang et al., 2002; Yuan et al., 2020a; 2020b). This was done in three steps: (i) from among all the collinear tracks, the track with the maximum number of observations was selected as the reference track; (ii) the SSH at each point on the collinear tracks corresponding to the point on the reference track was calculated by collinear analysis (Cheney et al., 1983; Wang and Rapp, 1992); (iii) the time-averaged SSH was calculated by averaging the SSH of the points on the collinear tracks. A mean track was thus obtained.

Collinear adjustment is well-suited for the correction of the ERM data for temporal variation, but it cannot be applied to the GM data. Fortunately, our datasets contained ERM data (that could be corrected for ocean variability) from one or more missions with the same observation period as that of the GM data (Table 1). The observations derived from different altimeter satellites during the same observation period were considered to have the same ocean variability. Sea level anomalies in the ERM data (e.g., T/P) were then used as a reference, to correct ocean variability of the GM data (e.g., ERS-1/GM).

The objective analysis method was used for the correction of the GM data for temporal variation. This method uses a priori statistical knowledge of the signal-data noise covariance functions (Le Traon et al., 1998). In this study, we applied a global suboptimal space/time objective analysis that considered along-track correlated errors (Le Traon et al., 1998; Ducet et al., 2000). To correct a GM data point for ocean variability, we initially selected the reference data points in a large subdomain with a space and time scale of 1000 km and 10 days, respectively. From among these data points, a smaller subdomain was then selected, comprising data points with the typical space scale of ocean signals (approximately 200–300 km) (Le Traon et al., 1998). Outside this smaller subdomain, only one in three to five data points was retained (Le Traon et al., 1998). This objective analysis method has been applied successfully for the determination of MSS models, such as models CLS11 and CLS15. More details on this method are provided in the literature (Le Traon et al., 1998; Ducet et al., 2000; Le Traon and Dibarboure, 2004).

3.2.2. Crossover adjustment

The long-wave ocean variation signals, such as part of the radial orbit error and seasonal ocean variations, were reduced after the correction of the ERM and GM data for ocean variability. However, many residuals remained including the residual radial orbit error, low-frequency sea level signals, and residual geophysical corrections. These residuals resulted in different SSHs on different tracks at the same location. Moreover, these residuals were further reduced with the application of the crossover adjustment method.

The crossover adjustment is a general method for integrating multi-satellite mission data (Huang et al., 2008). In conventional crossover adjustment, the radial orbit error is regarded as one of the main error sources affecting altimeter data, and is modelled adequately by either a time- or a distance-dependent polynomial (Huang et al., 2008; Yuan et al., 2020a). However, the process of solving the equation system in conventional crossover adjustment is complicated by a rank deficiency problem, and the computational procedure is complex and cumbersome (Huang et al., 2008). Moreover, in this study, the radial orbit error was of a magnitude similar to that of other physical and geometric uncertainties, such as the inconsistency of the satellite orbit frame and the additional error due to the residual ocean variation and geophysical corrections. To address these limitations, Huang et al (2008) modified the conventional crossover adjustment method by dividing it into two steps: (i) condition adjustment method, and, (ii) filtering and predicting of the observational corrections along each track. This modified crossover adjustment is described in detail by Huang et al (2008) and Yuan et al (2020a).

To better reflect the combined effect of the various sources of error

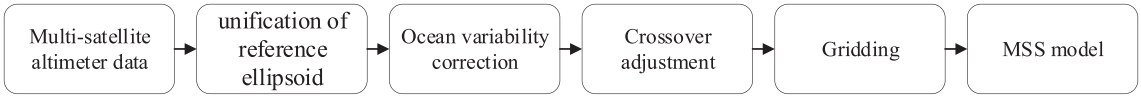

Fig. 2. Data processing procedures for establishing the MSS model.

Table 1
ERM data used for the correction of the GM data for temporal variation.

GM data			Corresponding ERM data		
Satellite	Cycles	Observation period	Satellite	Cycles	Observation period
ERS-1/GM	030–040	1994.04.10–1995.03.21	T/P	057–093	1994.04.01–1995.04.03
Jason-1/GM	500–537	2012.05.07–2013.06.21	Jason-2	140–183	2012.04.20–2013.06.30
HY-2A/GM	118–270	2016.03.30–2019.12.30	Jason-3	004–143	2016.03.18–2020.01.05
SRL/DP	100–135	2016.07.04–2019.12.16	Jason-3	014–142	2016.06.25–2019.12.26
Cryosat-2	014–125	2011.01.28–2019.12.12	Jason-2	094–303	2011.01.20–2016.10.02
			Jason-3	024–141	2016.10.02–2019.12.16

(radial orbit error, residual ocean variation, and residual geophysical corrections) on the altimeter data, an error model (form with a general polynomial and a trigonometric polynomial) was used to simulate these errors. The model is expressed as follows:

$$f(t) = a_0 + a_1 \cdot (t - T_s) + \sum_{j=1}^{m} (b_i \cdot cos(j \cdot \omega \cdot (t - T_s)) + c_i sin(j \cdot \omega \cdot (t - T_s))) \quad (1)$$

where t is the time of observation; a_0, a_1, b_i, and $c_i (i = 1, \cdots m)$ are model parameters to be solved; ω represents the angular frequency corresponding to the duration of a surveying track ($\omega = 2 \cdot \pi / (T_s - T_e)$, where T_s and T_e represent the start and end times of the surveying track, respectively); and m is a positive integer determined by the length of the track. Based on empirical evidence, m is proposed to be 1–2 for a short track, 3–5 for a middle-long track, and 6–8 for a long track (Huang et al., 2008; Yuan et al., 2020a).

3.2.3. Gridding

Gridding interpolatesis irregular altimeter data onto a regular grid. The least-squares collocation (LSC) technique (Hwang, 1989; Rapp and Bašić, 1992), proven to be the most suitable method (Jin et al., 2011), was used in this study. This technique considers the prior statistical information on the altimeter observations, which is crucial for the accurate interpolation of a grid point. In this study, the local LSC prediction method assumed a two-dimensional isotropic covariance function, described by the second-order Markov function (Jordan, 1972; Moritz, 1978):

$$D(d) = D_0 \cdot (1 + d/\alpha) \cdot e^{-d/\alpha} \quad (2)$$

where d is the two-dimensional distance between the prediction point and computation point, D_0 is the signal variance, and α is the correlation length (where a 50% correlation is obtained).

3.3. SLT model construction

A separate MSS model on a $1' \times 1'$ grid was established for each of the nine altimeter data groups (Fig. 1), and nine MSS models were result obtained. The fundament of each model was the mean along-track SSHs of the uninterrupted joint T/P series over different periods—for instance, from January 1993 to December 2011 for the Group1 model, and from January 1994 to December 2012 for the Group2 model. In this way, the fundament of each model was separated by one year with one year of ocean variability information between contiguous models. Therefore, the SSHs of grid points at the same position in these nine MSS models formed a time series with nine values, namely, $\{ssh_{i,j}\}, j = \{1, \cdots, 9\}$, where i was the i-th grid point in the Group j model. A linear regression equation was used to calculate the SLT at each grid point, as follows:

$$ssh_{i,j} = B_i + R_i * j \quad (3)$$

where B_i is the constant term of the SSH series at grid point i, andR_i is the SLT at grid point i, which can be solved using the least-squares method. The SLT model with a $1' \times 1'$ grid was thus obtained.

The estimations of our SLT model for different grid dimensions and datasets (Fig. 3) were mapped with Generic Mapping Tools (GMT: Wessel et al., 2019).

4. Results and discussion

The obtained SLT model is shown in Fig. 3(a). Fig. 3(a), (b), (c), and (d) show the SLT on a grid of $1' \times 1'$, $15' \times 15'$, $30' \times 30'$, and $60' \times 60'$, respectively. The SLT shown in Fig. 3(b) was calculated from the delayed-time, gridded ($15' \times 15'$ on a Cartesian grid) monthly mean of sea level anomalies product (AVISO) from January 1993 to September 2019. The SLTs in Fig. 3(c) and (d) were produced by NOAA and CSIRO, respectively, from the T/P and Jason-1/2/3 altimeter data over December 1992–September 2020 and January 1993–December 2019, respectively. Fig. 3(a), (b), (c), and (d) show that sea level does not change uniformly across the ocean. The characteristics of the SLT are the same in all four figures, but a higher-resolution grid, such as that in Fig. 3(a), reveals the spatial variabilities of the SLT in greater detail.

As shown in Fig. 3(a), the rate of SLR in the northern East China Sea (ESC) during the period of observation increased. This is attributed to the significant warming of the northern ESC (Fig. 4) (Tang et al., 2009; Yeh and Kim, 2010) due to the combined effect of the variability of the Kuroshio and the climate system, as well as the cooling of the coastal waters adjacent to the Changjiang River Estuary (Tang et al., 2009). As shown in Fig. 3(a), (b), and (c), a sea level change dipole was detected south of Japan. This is mainly attributed to the intensification of recirculation (Wang and Wu, 2019: Figure S2). A zonal SLT pattern occurred in the region of the North Pacific Subtropical Counter Current (STCC: an eastward current located in the band of 19.5°–22.5°N, populated with eddies) (Chang and Oey, 2014; Wang and Wu, 2018), and also east of Taiwan, and east of Luzon Island. This pattern is attributed to the chang in oceanic mesoscale eddies. Anticyclonic eddies contain warm water, which increases seawater volume and thus raises the sea level (the steric effect), resulting in a higher SLT. In contrast, cyclonic eddies contain cool water, which reduces the SLT. In the period of observation, the number of anticyclonic eddies increased yearly along the STCC and east of Luzon Island, and decreased east of Taiwan (Wang and Wu, 2018). This explains the high rate of SLR in the STCC and east of Luzon Island, and the zero to negative rate of SLR east of Taiwan. Near Xiasha, in the western South China Sea (SCS), the higher rate of SLR (6.26 mm/yr) may be caused by the higher frequent of anomalous anticyclonic (warm) eddies due to a shift in the SCS circulation system, driven by climate change (Xiao et al., 2020).

Sea level change mainly consists of two components, namely, steric (due to changes in ocean temperature and salinity) and mass components (Mu et al. 2019). Fig. 4(a) shows the steric SLT during January 1993–December 2019 (on a $60' \times 60'$ grid) calculated from EN4 quality-controlled ocean data (EN.4.2.1: Good et al., 2013) with Gouretski and Reseghetti bias correction (for details on the calculation method, see Gouretski and Reseghetti (2010), Llovel et al. (2013), and Llovel and Lee (2015)). The SLT characteristics in Fig. 4(a) are the same as those in Fig. 3. Fig. 4(b) shows the mass SLTs (on a $60' \times 60'$ grid) obtained from the SLTs of Fig. 3(a) minus the steric SLTs.

The mean rate of SLR in different waters within the study region was

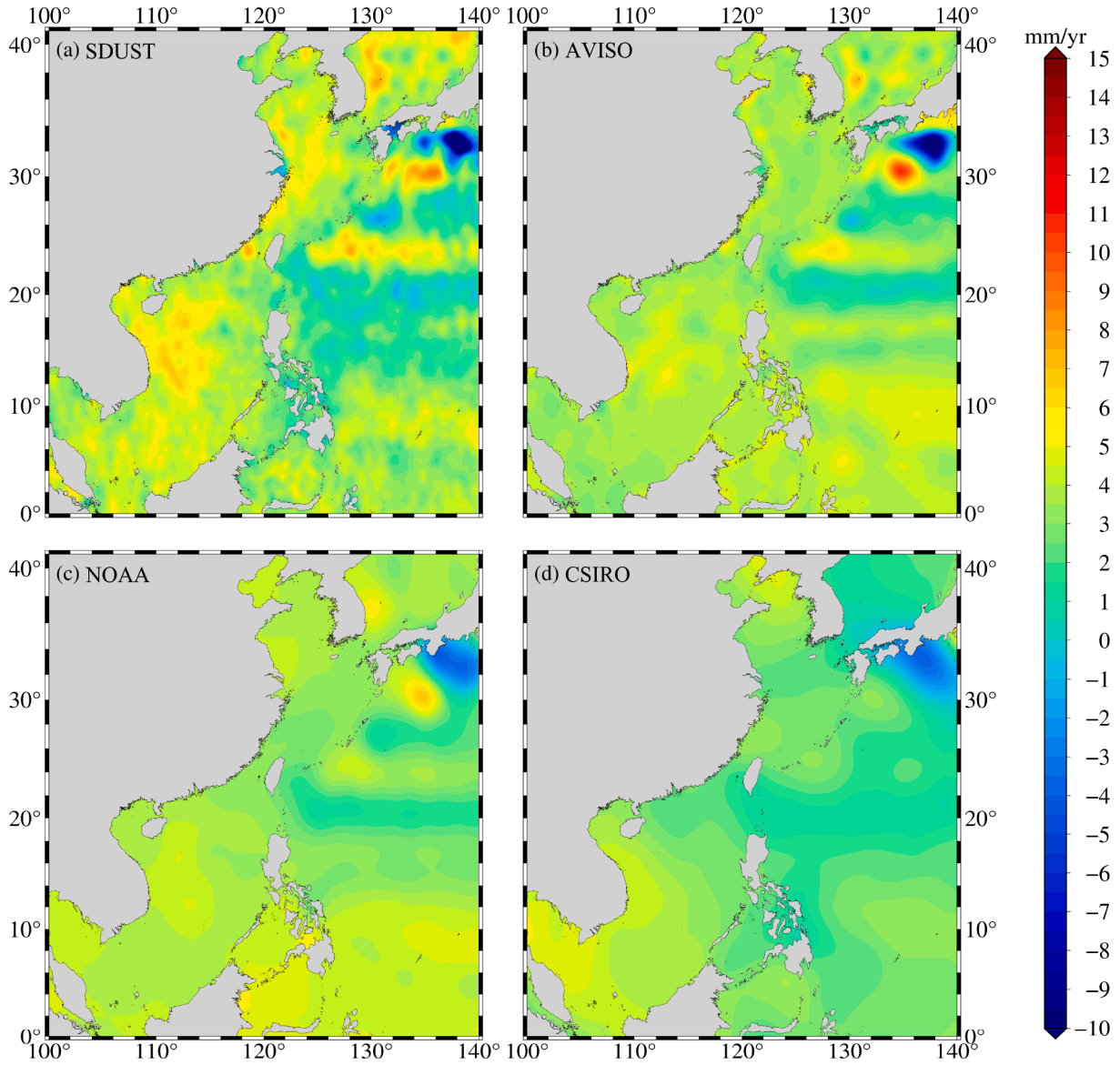

Fig. 3. SLT models in the China seas and their adjacent ocean. (a) Developed in this study (Shandong University of Science and Technology: SDUST) (Grid: 1′×1′; Period: January 1993–December 2019); (b) Calculated from the delayed-time gridded monthly mean of sea level anomalies product (AVISO) (Grid: 15′×15′; Period: January 1993–September 2019); (c) NOAA Laboratory for Satellite Altimetry (Grid: 30′×30′; Period: December 1992–September 2020); (d) CSIRO (Grid: 60′×60′; Period: January 1993–December 2019).

estimated from the data produced by different processing groups, as listed in Table 2. These results (not including CSIRO) were generally higher than 3.0 mm/yr—the rate of GMSL rise between 66° N and 66° S from 1993 to 2020, calculated by the NOAA Laboratory for Satellite Altimetry from T/P series data. Once again, our results confirm that SLTs vary across different seas. It should be noted that not all the estimates of SLR include effects of glacial isostatic adjustment on the geoid, which are estimated to be between + 0.2 and + 0.5 mm/yr globally (Peltier, 2004).

In the CSO, the mean rate of SLR calculated from our model was 3.42 mm/yr, consistent with the rate estimated from the AVISO and NOAA data, and slightly faster than that estimated from the CSIRO data (2.55 mm/yr). The mean rate of SLR in the Bohai Sea (BS: 117.5°–122°E, 37°–41°N), Yellow Sea (YS: 119°–123°E, 34°–38°N), ECS (117°–130°E, 23°–31°N), and SCS (105°–120°E, 3°–23°N) were 3.96, 4.29, 4.02, and 4.45 mm/yr, respectively. These values were slightly higher than those calculated from the data provided by AVISO, NOAA, and CSIRO. Moreover, the mean rate of SLR in the Xisha (XIW) and Nansha (NIW) islands waters were 6.26 and 4.52 mm/yr, respectively. These values were higher than those estimated from the AVISO, NOAA, and CSIRO data.

We also calculated the SLT in the offshore zone and the open ocean (Fig. 5), the lines 20–100 km away from the coastline used as the boundaries, respectively. The rate of SLR in the offshore zone was found to be approximate 0.67 mm/yr (~ 20%) higher than that in the open ocean. This finding is highly significant for the estimation of costal destruction—especially in coastal cities—due to SLR.

5. Conclusions

Most studies of sea level change rely on time series of the global average sea level. In this study, a new method for estimating the sea level change in the China seas and their adjacent ocean is proposed, and an SLT model with a 1′×1′ grid is developed. This high-resolution model, based on the time-varying MSS derived from several MSS models that incorporate multi-satellite altimeter data over different

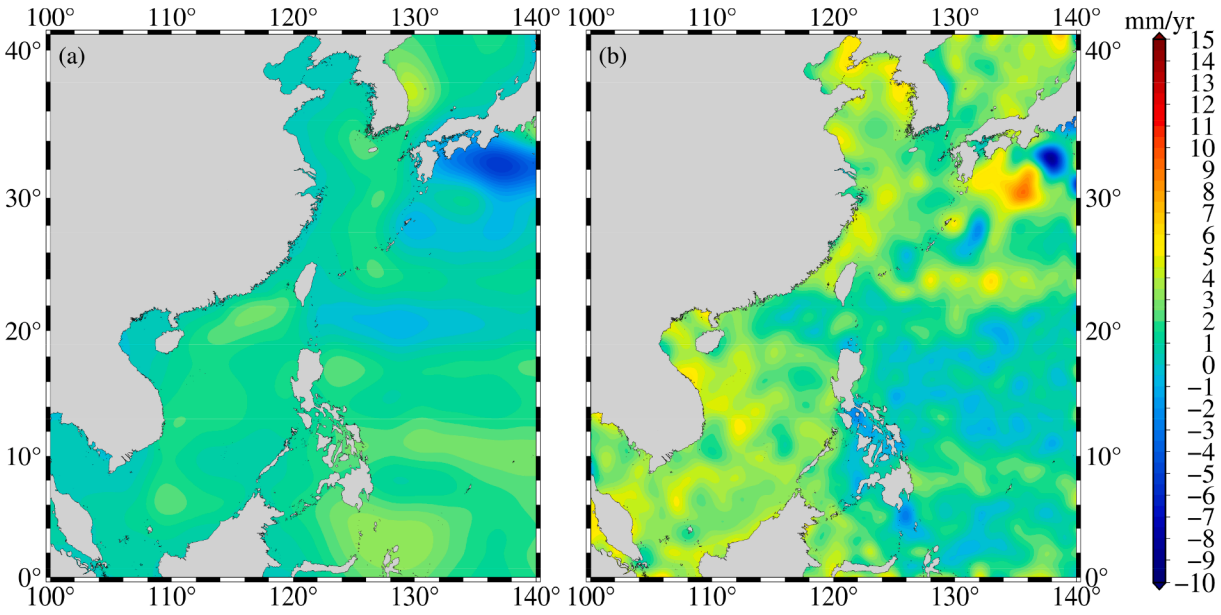

Fig. 4. Steric and mass SLTs in the China seas and their adjacent ocean. (a) Steric SLTs from EN4 quality-controlled ocean data (EN.4.2.1) (Grid: 60′×60′; Period: January 1993–December 2019); (b) Mass SLTs from the SLTs of Fig. 3 (a) minus the steric SLTs (Grid: 60′×60′; Period: January 1993–December 2019).

Table 2
Mean rate of sea level rise in different waters (mm/yr).

Areas	CSO	BS	YS	ESC	SCS	XIW	NIW
This stduty	3.42	3.96	4.29	4.02	4.45	6.26	4.52
AVISO	3.50	3.87	3.92	3.58	3.80	4.45	3.79
NOAA	3.54	4.20	3.98	3.11	3.90	4.48	3.96
CSIRO	2.55	3.95	3.40	2.61	3.33	3.50	3.65

periods of observation, reveals the sea level change in the study region in great detail.

The SLT model demonstrates that sea level does not change uniformly across the China seas and their adjacent ocean. This observation is of great significance for understanding the mechanisms of regional sea level change. Notable patterns of sea level change in the study region include a sea level change dipole south of Japan and a zonal SLT pattern appears in the STCC region, east of Taiwan, and east of Luzon Island. This differentiation of SLTs across the study region is attributed to changes in oceanic mesoscale eddies, a discordant Kuroshio (Wang and Wu, 2018) and variability in the climate system.

The rate of SLR in the China seas and their adjacent ocean is 3.42 mm/yr—higher than the global mean rate of approximately 3 mm/year. Moreover, within this region, the rate of SLR varies, from 3.96 mm/yr in the Bohai Sea, to 4.29, 4.02, and 4.45 mm/yr in the Yellow, East China, and the South China Sea, respectively. In the Xisha and Nansha island waters, sea level rises at a rate of 6.33 and 4.59 mm/yr, respectively.

We also found that the rate of SLR in the offshore zone is approximately 0.67 mm/yr (~ 20%) higher than that in the open ocean. This result is of great significance for the prevention of coastal destruction due to SLR.

CRediT authorship contribution statement

Jiajia Yuan: Data curation, Methodology, Resources, Visualization, Writing - original draft, Writing - review & editing. **Jinyun Guo:** Conceptualization, Methodology, Validation, Writing - review & editing. **Chengcheng Zhu:** Data curation, Validation, Visualization, Writing - review & editing. **Cheinway Hwang:** Validation, Visualization, Writing

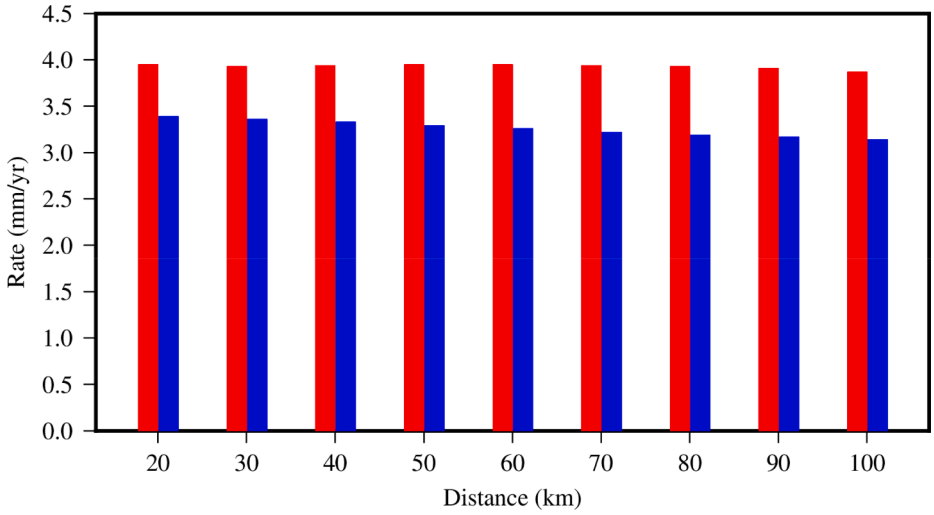

Fig. 5. Rate of sea level rise in the offshore (in red) and open ocean (in blue) with the lines 20–100 km away from the coastline used as the boundaries, respectively.

- review & editing. **Daocheng Yu:** Validation, Visualization, Writing - review & editing. **Mingzhi Sun:** Validation, Visualization, Writing - review & editing. **Dapeng Mu:** Validation, Visualization, Writing - review & editing.

Declaration of Competing Interest

The authors declare that they have no known competing financial interests or personal relationships that could have appeared to influence the work reported in this paper.

Acknowledgements

We are very grateful to AVISO for providing the along-track Level-2+ (L2P) products and the delayed-time gridded monthly mean of sea-level anomalies product, these are available from the website https://www.aviso.altimetry.fr/en/data/products/sea-surface-height-roducts/global/along-track-sea-level-anomalies-l2p.html and https://www.aviso.altimetry.fr/en/data/products/sea-surface-height-products/global/gridded-sea-level-anomalies-mean-and-climatology.html, respectively. We are also very grateful to the NOAA Laboratory for Satellite Altimetry and CSIRO for providing the sea level trends model on a grid of 30′×30′ and 60′×60′, respectively, these are available from the website https://www.star.nesdis.noaa.gov/socd/lsa/SeaLevelRise/LSA_SLR_maps.php and http://www.cmar.csiro.au/sealevel/sl_data_cmar.html. The EN4 quality controlled ocean data (EN.4.2.1) is available as described in Good et al. (2013). This work was supported by the National Natural Science Foundation of China (grant nos. 41774001, 41374009); and by the SDUST Research Fund (grant no. 2014TDJH101).

References

Andersen, O.B., Piccioni, G., Stenseng, L., Knudsen, P., 2016. The DTU15 MSS (mean sea surface) and DTU15LAT (lowest astronomical tide) reference surface. Proceedings of the ESA Living Planet Symposium 2016.

Andersen, O.B., Knudsen, P., Stenseng, L., 2018. A new DTU18 MSS mean sea surface–improvement from SAR altimetry, 25 Years of Progress in Radar Altimetry Symposium, Portugal. ftp://ftp.spacecenter.dk/ pub/DTU18/MSS_MATERIAL/PRESENTATIONS.

Cheney, R.E., Marsh, J.G., Beckley, B.D., 1983. Global mesoscale variability from collinear tracks of SEASAT altimeter data. J. Geophys. Res.-Oceans 88 (C7), 4343–4354. https://doi.org/10.1029/JC088iC07p04343.

Church, J.A., Gregory, J.M., Huybrechts, P., Kuhn, M., Lambeck, K., Nhuan, M.T., Qin, D., Woodworth, P.L., 2001. Changes in sea level. In: Houghton, J.T., Ding, Y., Griggs, D.J., Noguer, M., van der Linden, P.J., Dai, X., Maskell, K., Johnson, C.A. (Eds.), Climate change 2001: the scientific basis. Contribution of Working Group I to The Third Assessment Report of The Intergovernmental Panel on Climate Change. Cambridge University Press, pp. 639–693.

Cazenave, A., Dieng, H.-B., Meyssignac, B., Schuckmann, K.V., Decharme, B., Berthier, E., 2014. The rate of sea-level rise. Nat. Clim. Change 4 (5), 358–361. https://doi.org/10.1038/Nclimate2159.

Chang, Y.L., Oey, L.Y., 2014. Instability of the North Pacific Subtropical Countercurrent. J. Phys. Oceanogr. 44 (3), 818–833. https://doi.org/10.1175/JPO-D-13-0162.1.

Church, J.A., White, N.J., 2006. A 20th century acceleration in global sea-level rise. Geophys. Res. Lett. 33 (1), L01602. https://doi.org/10.1029/2005gl024826.

CNES, 2017. Along-track level-2+ (L2P) SLA product handbook. SALPMU-P-EA-23150-CLS, Issue 1.0. https://www.aviso.altimetry.fr/fileadmin/documents/data/tools/hdbk_L2P_all_missions_except_S3.pdf.

Ducet, N., Le Traon, P.Y., Reverdin, G., 2000. Global high-resolution mapping of ocean circulation from TOPEX/Poseidon and ERS-1 and -2. J. Geophys. Res.-Oceans 105 (C8), 19477–19498. https://doi.org/10.1029/2000jc900063.

Elipot, S., 2020. Measuring Global Mean Sea Level Changes With Surface Drifting Buoys. Geophys. Res. Lett. 47 (21) https://doi.org/10.1029/2020gl091078 e2020GL091078.

Guo, J., Wang, J., Hu, Z., Hwang, C., Chen, C., Gao, Y., 2015. Temporal-spatial variations of sea-level over China seas derived from altimeter data of TOPEX/Poseidon, Jason-1 and Jason-2 from 1993 to 2012. Chinese J. Geophys.-Ch. 58 (9), 3103–3120. https://doi.org/10.6038/cjg20150908.

Good, S.A., Martin, M.J., Rayner, N.A., 2013. EN4: quality controlled ocean temperature and salinity profiles and monthly objective analyses with uncertainty estimates. J. Geophys. Res.-Oceans 118, 6704–6716. https://doi.org/10.1002/2013JC009067.

Gouretski, V., Reseghetti, F., 2010. On depth and temperature biases in bathythermograph data: Development of a new correction scheme based on analysis of a global ocean database. Deep.-Sea. Res. Pt. I. 57, 812–833. https://doi.org/10.1016/j.dsr.2010.03.011.

Hwang, C.W., 1989. High Precision Gravity Anomaly and Sea Surface Height Estimation from Geos-3/Seasat Altimeter Data. M.S. Thesis. The Ohio State University, Columbus, OH, USA.

Huang, M., Zhai, G., Ouyang, Y., Lu, X., Liu, C., Wang, R., 2008. Integrated data processing for multi-satellite missions and recovery of marine gravity field. Terr. Atmos. Ocean. Sci. 19 (1–2), 103–109. https://doi.org/10.3319/TAO.2008.19.1-2.103(SA).

Intergovernmental Panel on Climate Change, 2014. Climate Change 2013: The Physical Science Basis, Cambridge Univ. Press, Cambridge, U. K., and New York.

Jiang, W., Li, J., Wang, Z., 2002. Determination of global mean sea surface WHU2000 using multi-satellite altimetric data. Sci. Bull. 47 (19), 1664–1668. https://doi.org/10.1007/bf03184119.

Jin, T., Li, J., Jiang, W., 2016. The global mean sea surface model Whu 2013. Geodesy and Geodynamics 7 (3), 202–209. https://doi.org/10.1016/j.geog.2016.04.006.

Jin, T., Li, J., Jiang, W., Wang, Z., 2011. The new generation of global mean sea surface height model based on multi-altimetric data. Acta Geodaetica et Cartographica Sinica 40 (6), 723–729.

Jordan, S.K., 1972. Self-consistent statistical models for the gravity anomaly, vertical deflections, and undulation of the geoid. J. Geophys. Res. 77 (20), 3660–3670. https://doi.org/10.1029/JB077i020p03660.

Le Traon, P.Y., Dibarboure, G., 2004. An Illustration of the Contribution of the TOPEX/Poseidon—Jason-1 Tandem Mission to Mesoscale Variability Studies. Mar. Geod. 27 (1–2), 3–13. https://doi.org/10.1080/01490410490489313.

Le Traon, P.Y., Nadal, F., Ducet, N., 1998. An improved mapping method of multisatellite altimeter data. J. Atmos. Ocean. Tech. 15 (2), 522–534. https://doi.org/10.1175/1520-0426(1998)015<0522:aimmom>2.0.co;2.

Llovel, W., Fukumori, I., Meyssignac, B., 2013. Depth-dependent temperature change contributions to global mean thermosteric sea level rise from 1960 to 2010. Global. Planet. Change 101, 113–118. https://doi.org/10.1016/j.gloplacha.2012.12.011.

Llovel, W., Lee, T., 2015. Importance and origin of halosteric contribution to sea level change in the southeast Indian Ocean during 2005–2013. Cont. Shelf. Res. 42, 1148–1157. https://doi.org/10.1002/2014GL062611.

Moritz, H., 1978. Least-squares collocation. Rev. Geophys. 16 (3), 421–430. https://doi.org/10.1029/RG016i003p00421.

Mu, D., Yan, H., 2018. The instantaneous rate of global mean sea-level rise. Chinese J. Geophys.-Ch. 61 (12), 4758–4766. https://doi.org/10.6038/cjg2018L0482.

Mu, D., Xu, T., Xu, G., 2019. Detecting coastal ocean mass variations with GRACE mascons. Geophys. J. Int. 217 (3), 2071–2080. https://doi.org/10.1093/gji/ggz138.

Nicholls, R.J., Cazenave, A., 2010. Sea-level rise and its impact on coastal zones. Science 328 (5985), 1517–1520. https://doi.org/10.1126/science.1185782.

Nicholls, R.J., Marinova, N., Lowe, J.A., Brown, S., Vellinga, P., de Gusmão, D., Hinkel, J., Tol, R.S.J., 2011. Sea-level rise and its possible impacts given a beyond 4 C world in the twenty-first century. Philos. T. R. Soc. A. 369 (1934), 161–181. https://doi.org/10.1098/rsta.2010.0291.

Niu, Y., Guo, J., Yuan, J., Zhu, C., Zhou, M., Liu, X., Ji, B., 2020. Prediction of sea level change in Japanese coast using singular spectrum analysis and autoregression moving average. Chinese J. Geophys.-Ch. 63 (9), 3263–3274. https://doi.org/10.6038/cjg2020N0203.

Peltier, W.R., 2004. Global Glacial Isostasy and The Surface of The Ice-Age Earth: The Ice-5g (Vm2) Model and Grace. Annu. Rev. Earth. Pl. Sc. 20 (32), 111–149. https://doi.org/10.1146/annurev.earth.32.082503.144359.

Pujol, M.-I., Schaeffer, P., Faugère, Y., Raynal, M., Dibarboure, G., Picot, N., 2018. Gauging the improvement of recent mean sea surface models: A new approach for identifying and quantifying their errors. J. Geophys. Res.-Oceans 123 (8), 5889–5911. https://doi.org/10.1029/2017JC013503.

Rapp, R.H., Bašić, T., 1992. Oceanwide gravity anomalies from GEOS-3, Seasat and Geosat altimeter data. Geophys. Res. Lett. 19 (19), 1979–1982. https://doi.org/10.1029/92GL02247.

Rapp, R.H., Yi, Y., Wang, Y.M., 1994. Mean sea surface and geoid gradient comparisons with TOPEX altimeter data. J. Geophys. Res.-Oceans 99 (C12), 24657–24667. https://doi.org/10.1029/94jc00918.

Schaeffer, P., Faugére, Y., Legeais, J.F., Ollivier, A., Guinle, T., Picot, N., 2012. The CNES_CLS11 Global Mean Sea Surface Computed from 16 Years of Satellite Altimeter Data. Mar. Geod. 35 (sup1), 3–19. https://doi.org/10.1080/01490419.2012.718231.

Tang, X., Wang, F., Chen, Y., Li, M., 2009. Warming trend in northern East China Sea in recent four decades. Chin. J. Oceanol. Limn. 27 (2), 185–191. https://doi.org/10.1007/s00343-009-9238-4.

Voosen, P., 2020. Seas are rising faster than ever. Science 370 (6519), 901. https://doi.org/10.1126/science.370.6519.901.

Watson, C.S., White, N.J., Church, J.A., King, M.A., Burgette, R.J., Legresy, B., 2015. Unabated global mean sea-level rise over the satellite altimeter eras. Nat. Clim. Change 5 (6), 565–568. https://doi.org/10.1038/nclimate2635.

Watson, P.J., 2016. A new perspective on global mean sea-level (GMSL) acceleration. Geophys. Res. Lett. 43 (12), 6478–6484. https://doi.org/10.1002/2016gl069653.

Wang, Y.M., Rapp, R.H., 1992. The determination of a one year mean sea surface height track from Geosat altimeter data and ocean variability implications. Bull. Géodésique 66 (4), 336–345. https://doi.org/10.1007/BF00807418.

Wang, Y.L., Wu, C.R., 2018. Discordant multi-decadal trend in the intensity of the Kuroshio along its path during 1993–2013. Sci. Rep.-Uk 8, 14633. https://doi.org/10.1038/s41598-018-32843-y.

Wang, Y.L., Wu, C.R., 2019. Enhanced warming and intensification of the Kuroshio extension, 1999–2013. Remote Sens.-Basel 11 (1), 101. https://doi.org/10.3390/rs11010101.

Wessel, P., Luis, J.F., Uieda, L., Scharroo, R., Wobbe, F., Smith, W.H.F., Tian, D., 2019. The Generic Mapping Tools Version 6. Geochem. Geophy. Geosy. 20 (11), 5556–5564. https://doi.org/10.1029/2019GC008515.

Xiao, F., Wang, D., Leung, Y.T., 2020. Early and extreme warming in the South China Sea during 2015/16: Role of an unusual Indian Ocean dipole event. Geophys. Res. Lett. 47 (17) https://doi.org/10.1029/2020GL089936 e2020GL089936.

Yeh, S.W., Kim, C.H., 2010. Recent warming in the Yellow/East China Sea during winter and the associated atmospheric circulation. Cont. Shelf. Res. 30 (13), 1428–1434. https://doi.org/10.1016/j.csr.2010.05.002.

Yuan, J., Guo, J., Liu, X., Zhu, C., Niu, Y., Li, Z., Ji, B., Ouyang, Y., 2020a. Mean sea surface model over China seas and its adjacent ocean established with the 19-year moving average method from multi-satellite altimeter data. Cont. Shelf. Res. 192 (1), 104009 https://doi.org/10.1016/j.csr.2019.104009.

Yuan, J., Guo, J., Niu, Y., Zhu, C., Li, Z., Liu, X., 2020b. Denoising effect of Jason-1 altimeter waveforms with singular spectrum analysis: A case study of modelling mean sea surface height over South China Sea. J. Mar. Sci. Eng. 8 (6), 426. https://doi.org/10.3390/jmse8060426.